FULL PAPER

Scissor Lift with Real-Time Self-Adjustment Ability Based on Variable Gravity Compensation Mechanism

Naoyuki Takesue[a*], Yosuke Komoda[a], Hideyuki Murayama[b], Kousyun Fujiwara[b], and Hideo Fujimoto[c]

[a] *Tokyo Metropolitan University, Hino, Japan*;
[b] *Toyota Motor Corporation, Toyota, Japan*;
[c] *Nagoya Institute of Technology, Nagoya, Japan*;

Most robots involved in vertical movement against gravitation require actuators large enough to support their own weight. To improve the inherent safety of such robots against the large actuators and reduce their energy consumption, numerous gravity compensation mechanisms (GCMs) have been proposed. Our previous study proposed a variable GCM (VGCM) that uses two types of springs and can adjust the compensation force. In this paper, a VGCM-based scissor lift (pantograph lift) that uses three springs and a smaller actuator is proposed. A prototype is designed and fabricated, and the performance of the prototype is evaluated experimentally. The results demonstrate that the developed scissor lift meets the design specifications. In addition, a load estimator is established based on the dynamic model of the scissor lift. A real-time self-adjustment method that automatically changes the compensation force is proposed, and its effectiveness is verified.

Keywords: Scissor Lift, Pantograph, Gravity Compensation Mechanism, Spring, Adjustable

1.   Introduction

Robots involved in vertical movement against gravitation require actuators large enough to support their own weight, although selective compliance assembly robot arm (SCARA) robots can support themselves structurally. When humans work with these robots, there is a risk that the large actuators may injure them. Therefore, to improve the inherent safety of these robots and minimize their energy consumption, mechanisms capable of compensating for gravity have been devised [1].

It is well known that there are two types of mechanical compensation methods [2]: mass balancing [3, 4] and spring balancing [5–22]. The spring balance has the advantage that the total weight of the system is not significantly increased.

Various approaches can be used for the spring balance, such as zero-free-length springs with links [5–9], springs with 1:2-ratio gears [10, 11], springs with noncircular pulleys [12, 13], and springs with cams [14]. A pantograph mechanism using a spring [15–17] is another such approach.

Pantograph lifts, which are also called scissor lifts, are widely used for the vertical transportation of load and assembly works in automotive factories [24–26]. Scissor lifts consume energy to maintain the table position. Therefore, a pantograph mechanism that generates a constant repulsive force has been proposed [15, 16]. This mechanism uses two types of springs that have positive and negative spring constants. The concept of springs with negative constant is often used in research on vibration isolation [27, 28]. Another type of gravity compensation mechanism

---

*Corresponding author. Email: ntakesue@tmu.ac.jp

(GCM) that uses springs and 1:2-ratio gears has been applied to a scissor lift for heavy works over 100 kg in [17].

Most GCMs can compensate a predetermined constant weight. Such GCMs fail to maintain balance with the gravitational force if the weight changes from the predetermined value in the design specifications or if the work mass varies widely. Therefore, some studies propose adjustable mechanisms [5, 18–23]. Although self-adjusting mechanisms were presented in [5], the adjustment mode is limited to only the preselected position. In [18], four concepts of energy-free adjustable mechanisms are described: simultaneous displacement [19], virtual springs [20], spring constant [21], and storage springs [22]. In [23], counterbalance systems including energy-free adjustment are classified into seven categories. Energy-free adjustment is useful for therapeutic and assistive applications. In many cases, however, during the adjustment, the weight arm and/or the compensation adjuster must be locked in a certain position. Therefore, the adjustment needs a sequential operation and it cannot be achieved immediately. For industrial applications, the adjustment should be done at an arbitrary position in a short time, although some energy may be allowed to compensate for a new payload.

Our previous study proposed a variable GCM (VGCM) that can adjust the compensation ratio of the load by varying the displacement (equilibrium) of the spring [29]. Our proposed VGCM uses two types of springs with a 90° phase difference in the same manner as in [16], but it is adaptable to variable gravity by deriving perfect balancing conditions. Once the compensation force is adjusted to balance the payload, the force required to move it up and down is very small. However, the force required to vary the compensation may not be small, especially if the displacement of the spring is large. Therefore, in this paper, a VGCM-based scissor lift that uses a third spring and a smaller actuator is proposed. It is considered to be a practical configuration because all of the springs are arranged in parallel at the bottom of the lift. Moreover, a real-time self-adjustment method for an arbitrary payload is presented. Since counterbalance systems with energy-free adjustment[18, 23] have to lock the weight arm and/or the compensation adjuster in a certain position during the adjustment, the real-time adjustment has not been shown.

The remainder of this paper is organized as follows. Section II briefly describes the principles of the VGCM using two springs A and B, and the VGCM-based scissor lift is proposed. In addition, to reduce the adjustment motor size, a third spring C is introduced. In Section III, the parameters for the scissor lift are designed and a prototype VGCM-based scissor lift is presented. Section IV describes various verification experiments. In Section V, load estimation performance and self-adjustment experiments are conducted based on the load estimation. Finally, in Section VI, we summarize this paper and propose future work.

2.   VGCM-Based Scissor Lift

2.1   Principles of VGCM

In this section, the principles of VGCM [29] are briefly described with reference to Fig. 1. It is assumed that a link pivots on point O. When the link is in the original position along the vertical line, as shown in Fig. 1 (a), the angle θ is zero. When the link rotates in the clockwise direction around point O, θ is defined as a positive angle. The gravitational force mg of the load is applied to the point G of the link, as shown in Fig. 1 (b). The torque τ_g generated by the gravitational force is written as

$$\tau_g = mgl_{\mathrm{G}} \sin \theta. \tag{1}$$

Regular (non-zero-free-length) springs A and B, which are oriented horizontally and vertically, respectively, are connected to the points A and B of the link, respectively, so that the spring

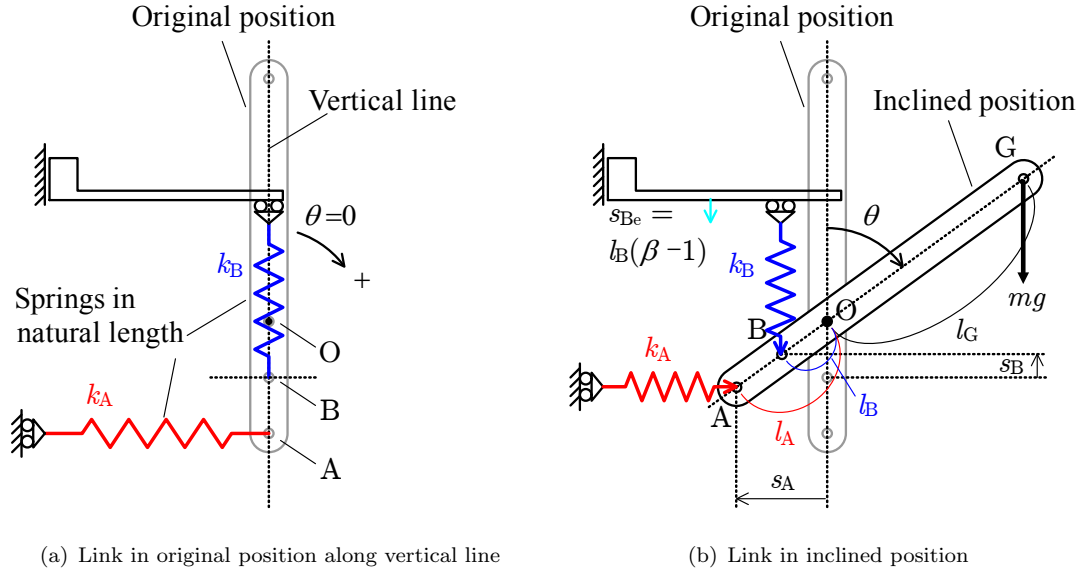(a) Link in original position along vertical line   (b) Link in inclined position

Figure 1. Schematic of variable gravity compensation mechanism (VGCM)

forces compensate the gravitational force. The spring forces are written as

$$f_A = -k_A s_A = -k_A l_A \sin\theta, \tag{2}$$

$$f_B = -k_B s_B = -k_B l_B (1 - \cos\theta), \tag{3}$$

where s_A and s_B are the horizontal and vertical displacements of springs A and B, respectively, from their original positions. Therefore, when the link is in the original position, the displacements s_A and s_B are both zero.

The torque produced by the springs is obtained as

$$\begin{aligned}
\tau_k &= \tau_{kA} + \tau_{kB} \\
&= f_A l_A \cos\theta + f_B l_B \sin\theta \\
&= -k_A l_A^2 \sin\theta \cos\theta - k_B l_B^2 (1 - \cos\theta) \sin\theta.
\end{aligned} \tag{4}$$

Assuming $k_A l_A^2 = k_B l_B^2 = W$, the spring torque τ_k can be rewritten as

$$\tau_k = -W \sin\theta. \tag{5}$$

If $W = mgl_G$, the total torque τ_{link} applied to the link is

$$\tau_{\text{link}} = \tau_g + \tau_k = mgl_G \sin\theta - W \sin\theta = 0. \tag{6}$$

This means that the spring torque is statically balanced with the gravitational torque.

Moreover, adding an initial displacement $s_{Be} = l_B(\beta - 1)$ to the other end of spring B, the spring torque is changed to

$$\begin{aligned}
\tau_k(\beta) &= -k_A s_A l_A \cos\theta - k_B (s_B + s_{Be}) l_B \sin\theta \\
&= -k_A l_A^2 \sin\theta \cos\theta - k_B l_B^2 (\beta - \cos\theta) \sin\theta \\
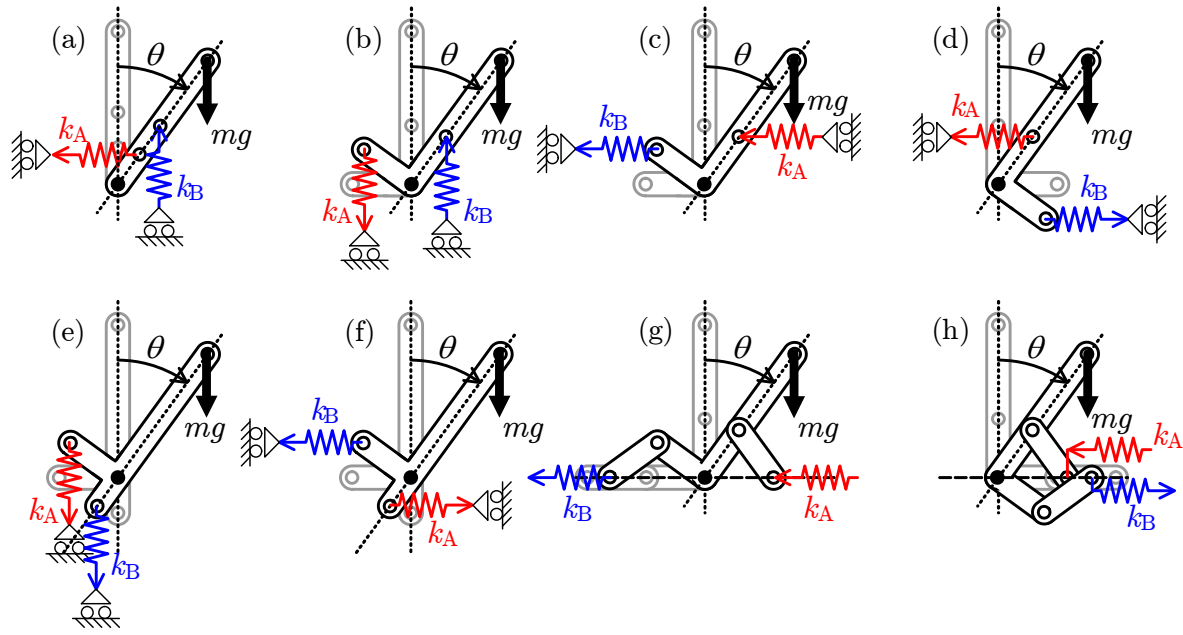&= -\beta W \sin\theta.
\end{aligned} \tag{7}$$

Figure 2. Configurations of the GCM

This means that the spring torque balances with the load weight multiplied by β. Therefore, adding an appropriate initial displacement to spring B can adjust the compensation force according to the change in the load.

2.2 VGCM-Based Scissor Lift

The explanation given in the previous section is based on the use of a straight link and two springs aligned perpendicular to each other (horizontally and vertically, respectively). Other configurations can be considered based on the same principle, as shown in Fig. 2. When the link is L-shaped as shown in Fig. 2 (b)–(f), it allows two springs to align in parallel direction. An additional link allows removing a slider, as shown in Fig. 2 (g) and (h).

To use the VGCM principle for a practical lift, we propose the scissor (pantograph) lift shown in Fig. 3, which is the similar configuration to Fig. 2 (h). The symbols in the figure represent the same quantities as in Fig. 1. In the scissor lift, the springs are aligned at the base of the lift.

In addition, motors for the lift and adjustment located at points O and B_{e}(the other end of spring B), respectively, are shown in Fig. 4. The motor for the lift should include appropriate gears. The motor for adjusting the compensation should be a linear drive, such as a screw. To hold the position, it may be preferable to be non-backdrivable.

By controlling the position of the adjustment motor, the compensation force from springs A and B can be changed, and the load of the lift motor can be reduced.

2.3 Addition of Spring C

Although increasing the displacement $s_{\mathrm{B}} + s_{\mathrm{Be}}$ of spring B increases the compensation force and reduces the load of the lift motor, this increase in the displacement simultaneously enlarges the drive force of the adjustment motor. In spite of the introduction of springs to reduce the required torque of the lift motor, a larger motor for adjustment is required, which is undesirable.

Therefore, we add spring C via a link mechanism, as shown in Fig. 5, assuming that the link length is $l_{\mathrm{C}}/2$ and the angle of the link is $0 < \phi < \pi/2$. Spring C is fixed so that its displacement
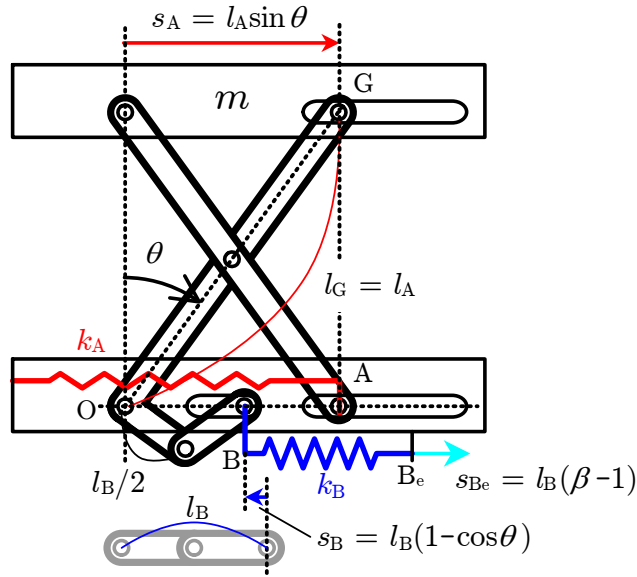
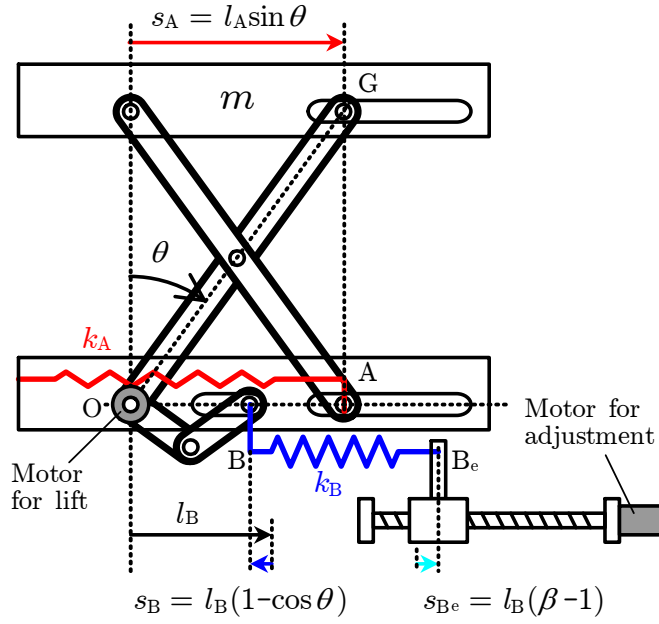Figure 3. Schematic of VGCM-based scissor lift

Figure 4. Schematic of VGCM-based scissor lift with motors

is zero when $\phi = \pi/2$. Then, the displacement can be written as

$$s_\mathrm{C} = -l_\mathrm{C} \cos \phi. \tag{8}$$

The displacement $s_{\mathrm{C}'}$ of point C' can be written as

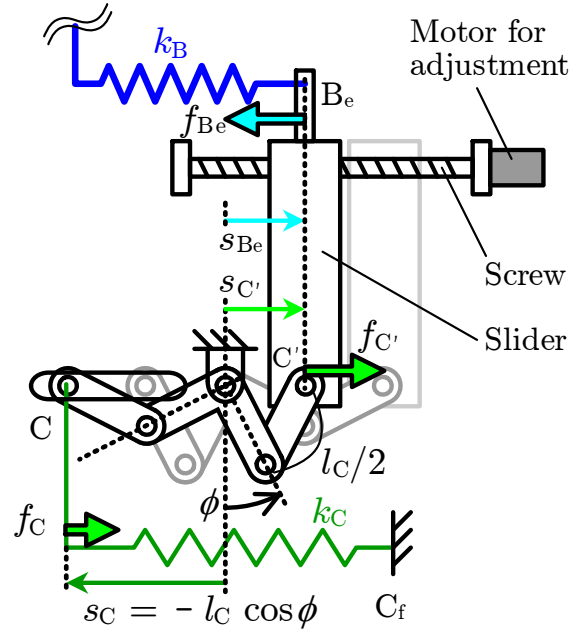$$s_{\mathrm{C}'} = l_\mathrm{C} \sin \phi. \tag{9}$$

Figure 5. Schematic of adjustment mechanism with spring C

The relationship between the two displacements in (8) and (9) can be derived as

$$\dot{s}_{C'} = J\dot{s}_C \tag{10}$$

where $J = \tan^{-1}\phi$ corresponds to the Jacobian.

The spring force f_C is applied at point C:

$$f_C = -k_C s_C = k_C l_C \cos\phi. \tag{11}$$

The spring force $f_{C'}$ at point C' is obtained as

$$f_{C'} = J^{-1} f_C = k_C l_C \sin\phi = k_C s_{C'}. \tag{12}$$

The forces f_{B_e} and $f_{C'}$ are applied to the slider driven by the adjustment motor. The total force is expressed as

$$f_{BC} = f_{B_e} + f_{C'} = -k_B(s_B + s_{B_e}) + k_C s_{C'}. \tag{13}$$

Here, assuming that $k_B = k_C$ and $s_{B_e} = s_{C'}$, the total force f_{BC} becomes $-k_B s_B$. Therefore, the total force does not depend on the position s_{B_e} of the slider, whereas it does depend on the position θ of the lift table because s_B is a function of θ.

In other words, the potential energy stored by spring C is utilized to pull spring B. As a result, the force of the adjustment motor that is required to move the equilibrium position of spring B is reduced.

3.   Prototype VGCM-based Scissor Lift

Based on the principle described in the previous section, a prototype scissor lift is developed.

6

3.1   *Parameter Design*

Assuming a lift table mass of $\bar{m} = 2$ kg and a link length of $l_\mathrm{G} = l_\mathrm{A} = 0.25$ m, the theoretical spring constant $\tilde{k}_\mathrm{A}$ of spring A can be obtained as

$$\tilde{k}_\mathrm{A} = \frac{\bar{m}gl_\mathrm{G}}{l_\mathrm{A}^2}$$

$$= \frac{2 \times 9.8 \times 0.25}{0.25^2} = 78.4 \text{ N/m}. \tag{14}$$

This spring constant is described as 'theoretical' because in practical situations, a physical spring with the calculated spring constant is not available in all cases. For the prototype, a spring whose constant is 40.6 N/m is chosen, and two substitute springs are utilized such that the total spring constant is $k_\mathrm{A} = 81.3$ N/m. As a result, when the displacement s_Be is zero, the spring force balances with the table mass, as $m = k_\mathrm{A}l_\mathrm{A}^2/(gl_\mathrm{G}) = 2.1$ kg, which is called the nominal mass in this paper.

Next, assuming a link length of $l_\mathrm{B} = 0.09$ m, the theoretical spring constant $\tilde{k}_\mathrm{B}$ of spring B is determined as

$$\tilde{k}_\mathrm{B} = \frac{k_\mathrm{A}l_\mathrm{A}^2}{l_\mathrm{B}^2}$$

$$= \frac{81.3 \times 0.25^2}{0.09^2} = 6.27 \times 10^2 \text{ N/m}. \tag{15}$$

Four substitute springs are used for spring B such that the spring constant is approximately $k_\mathrm{B} = 6.23 \times 10^2$ N/m. The springs that are utilized are the same as spring C.

It can be considered that the error between $\tilde{k}_\mathrm{B}$ and k_B may affect the balancing error. In this case, however, since the error ratio is $\varepsilon = (\tilde{k}_\mathrm{B} - k_\mathrm{B})/\tilde{k}_\mathrm{B} = 6.4 \times 10^{-3}$, the balancing error which will be compensated by the lift motor is less than 1 percent. The spring torque is

$$\tau_k(\beta) = -k_\mathrm{A}l_\mathrm{A}^2 \sin\theta \cos\theta - k_\mathrm{B}l_\mathrm{B}^2(\beta - \cos\theta) \sin\theta$$

$$= -(\tilde{k}_\mathrm{B} - k_\mathrm{B})l_\mathrm{B}{}^2 \sin\theta \cos\theta - \beta k_\mathrm{B}l_\mathrm{B}{}^2 \sin\theta$$

$$= -\varepsilon(\cos\theta - \beta)W \sin\theta - \beta W \sin\theta \tag{16}$$

where the first term is the balancing error torque and the second term is the adjustable spring compensation torque.

3.2   *Prototype*

Fig. 6 shows an overview of the developed VGCM-based scissor lift. Fig. 7(a)–(d) illustrates the details. Fig. 7(a) shows the front view of the scissor lift. Fig. 7(b) depicts the top view of the adjustment drive. Figs. 7(c) and 7(d) demonstrate the change in springs B and C for small and large s_Be, respectively. The lift table is backdrivable while the adjustment slider is non-backdrivable.

The specifications are listed in Table 1. Although the nominal mass was $m = 2.1$ kg in the design phase, the actual mass of the lift table was approximately 3 kg. Because the maximum displacement of spring B used in the prototype is $s_\mathrm{Bmax} = 0.27$ m, the range of the compensation mass is $\beta m = 2.1$ – 6.3 kg based on $\max(\beta) = s_\mathrm{Bmax}/l_\mathrm{B} = 0.27/0.09 = 3$. To balance the compensation force with the weight of the lift table, the displacement of spring B is adjusted to $s_\mathrm{Be} = 0.045$ m, which corresponds to $\beta = 1.5$, as the initial setting β_0. Therefore, the lift can balance additional weight of up to approximately 3.3 kg.
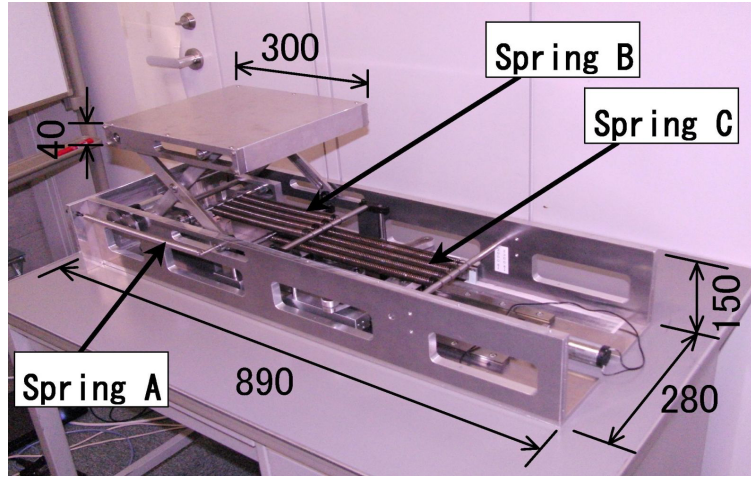
Figure 6. Overview of prototype VGCM-based scissor lift

Table 1. Specifications of VGCM-based scissor lift

Nominal mass m	2.1 kg
Adjustable compensation ratio β	$1 - 3$
Compensatable mass	$2.1 - 6.3$ kg
Actual table mass m_T	3 kg
Link length l_A, l_G	0.250 m
Link length l_B, l_C	0.090 m
Spring constant k_A	81.3 N/m (total of 2 springs)
Spring constant k_B, k_C	6.23×10^2 N/m (total of 4 springs)

Table 2. Specifications of motors

| Motor	Lift motor	Adjustment motor
Product	maxon A-max32	
Power	20 W	
Nominal voltage	12 V	
Nominal speed	3170 rpm	
Nominal torque	0.044 N·m	
Stall torque	0.140 N·m	
Encoder resolution	1024 ppr	
Gear ratio	1:198	1:4.8 & 2 mm lead screw

Two maxon motors A-max32 (20 W) are used as the lift and adjustment motors. The gear ratios for the lift and adjustment are 1:198 and 1:4.8, respectively. In addition, the adjustment drive is a trapezoidal screw with a 2 mm lead. Each motor has a rotary encoder whose resolution is 1024 ppr. The angle of lift motor is initialized by a potentiometer fixed on the axis of the scissor lift. The specifications of motors are listed in Table 2.
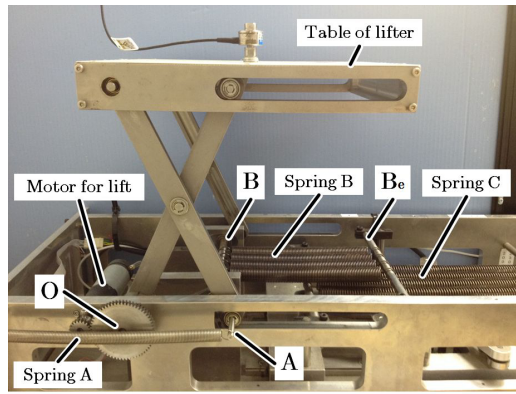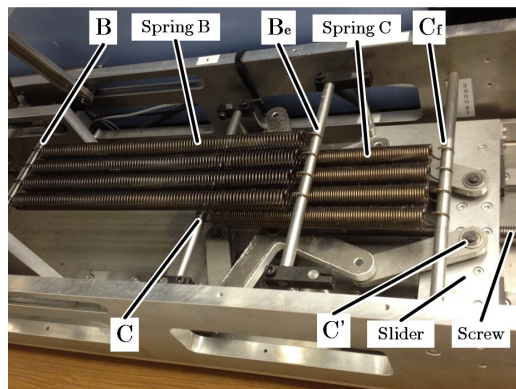
(a) Front view of scissor lift
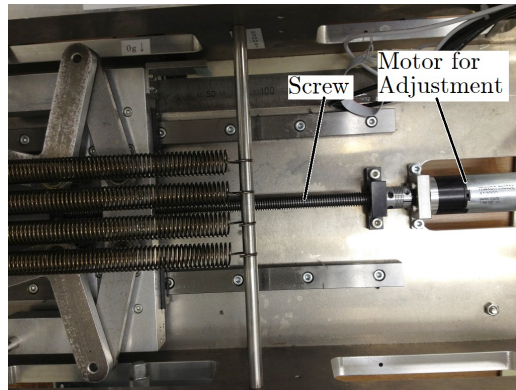
(b) Top view of adjustment motor
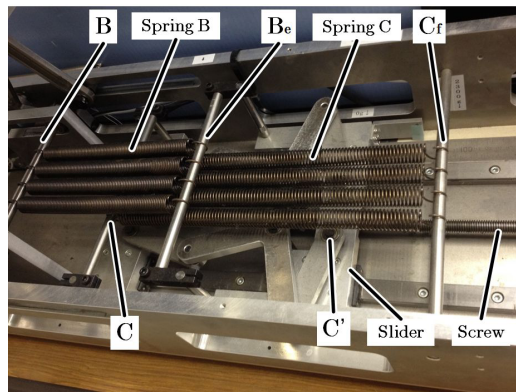
(c) Springs B and C in case of small s_{Be}

(d) Springs B and C in case of large s_{Be}

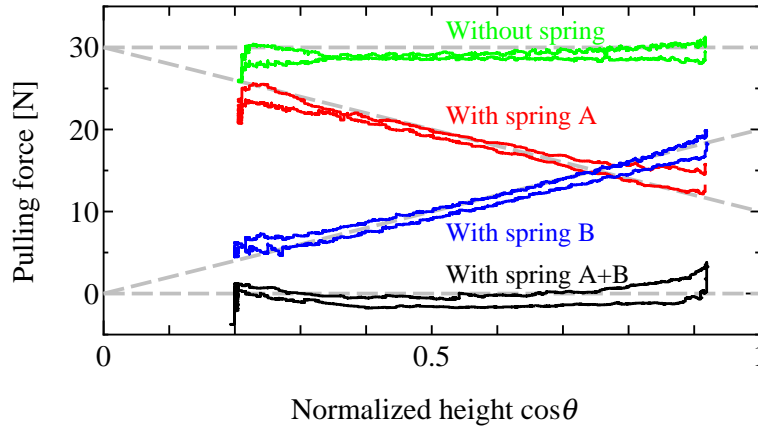Figure 7. Details of VGCM-based scissor lift

Figure 8. Pulling force vs. normalized height with no spring (green), only spring A (red), only spring B (blue), and both springs A and B (black)

4.   Verification Experiments

To verify the performance of the VGCM-based scissor lift, various experiments are conducted.

4.1   *Compensation Force by Springs*

In the first experiment, the compensation force of springs A and B is verified. A load cell is attached to the top of the lift. The lift motor is turned off, and the top of load cell is pulled up and down. The table height and the load cell force are measured.

The spring conditions are as follows:

(1) without springs,
(2) with only spring A,
(3) with only spring B,
(4) with both springs A and B.

In the case of no spring, the force of the load cell corresponds to the weight $m_{\mathrm{T}}g$ of the table. With any springs, the force of the load cell must be reduced by the compensation force of the springs.

The experimental results are shown in Fig. 8. The vertical axis indicates the pulling force measured by the load cell. The horizontal axis represents the normalized height $\cos\theta$ of the table. The green, red, blue, and black lines depict the results under conditions (1)–(4), respectively. The gray dashed lines denote the theoretical characteristics.

As shown in the figure, the gravitational force of the lift table including links was approximately 30 N (approximately 3 kgf). In the case of no spring (without compensation), the lift motor must support the entirety of the load. Conversely, it can be confirmed that the addition of spring A or B reduces the pulling force of the table.

With both springs A and B, the load is almost completely compensated. The absolute force is less than 2 N when the lift table is pulled up and down at any height. In this case, the energy of the lift motor will be reduced drastically, and the motor can be miniaturized.

4.2   *Motor Torque*

4.2.1   Lift motor with/without compensation

In the next experiment, the lift motor is turned on, and the position of the lift table is controlled under two conditions: without springs (no compensation) and with springs (compensation). A
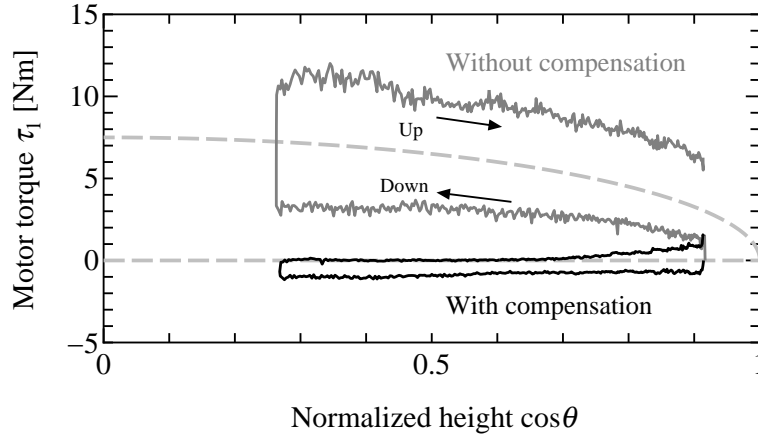
10

Figure 9. Lift motor torque vs. normalized height with and without compensation

proportional-derivative (PD) controller is employed using the following equation:

$$\tau_1 = K_P(\theta_d - \theta) + K_D(\dot{\theta}_d - \dot{\theta}) \tag{17}$$

where θ_d is the desired angle and K_P and K_D are the proportional and derivative gains, respectively. The motor torque is obtained from this command.

The motor torque is shown in Fig. 9. The vertical and horizontal axes represent the torque τ_1 of the lift motor and the normalized height $\cos\theta$ of the table, respectively.

When there is no compensation from the spring, when the height is close to zero, a motor torque of $m_T g \, l_G = 3 \times 9.8 \times 0.25 \simeq 7.4$ N·m is theoretically required. In the experiment, a large hysteresis was observed as a result of the friction of the drive system. A maximum torque of approximately 12 N·m was output when the table was lifted up. Conversely, the motor torque was within 1 N·m under spring compensation. In that case, the hysteresis was relatively small.

4.2.2   Adjustability of compensation

To evaluate the variability of the compensation, the displacement s_{Be} of the slider is changed, and the torque of the lift motor is measured.

The conditions are $s_{Be} = 45$, 90, 135 or 180 mm, which correspond to $\beta = 1.5$, 2.0, 2.5 or 3.0, respectively, and additional weights of 0, 1, 2 or 3 kg, respectively.

The experimental results are shown in Fig. 10. The gray solid lines indicate the motor torques under no additional weight ($m_W = 0$ kg) when β is set to 2.0, 2.5 or 3.0. The gray dashed lines show the theoretical values.

The black solid lines represent the case with an additional weight corresponding to β. In all cases, the motor torque is within 1 N·m even though a weight of 0, 1, 2 or 3 kg is added.

As shown in the results, the adjustability of the compensation resulting from changing the displacement s_{Be} or β was verified.

4.2.3   Adjustment motor

It is confirmed that the introduction of spring C reduces the adjustment motor torque.

The lift table is set to high ($\cos\theta = 0.92$), middle ($\cos\theta = 0.72$), and low ($\cos\theta = 0.33$) positions. The torque of the adjustment motor is measured when the displacement changes from $\beta = 1.5$ to $\beta = 2.8$ for 10 s.

Theoretical force to move the adjustment slider was expressed as (13). The theoretical forces are shown in Fig. 11. The vertical and horizontal axes indicate the adjustment force and the displacement β, respectively. The thin solid, thick broken, and thick solid lines depict the results with the lift table set to the high, middle, and low positions. As seen from the figure, it is expected that the required motor torque for the adjustment is effectively reduced.
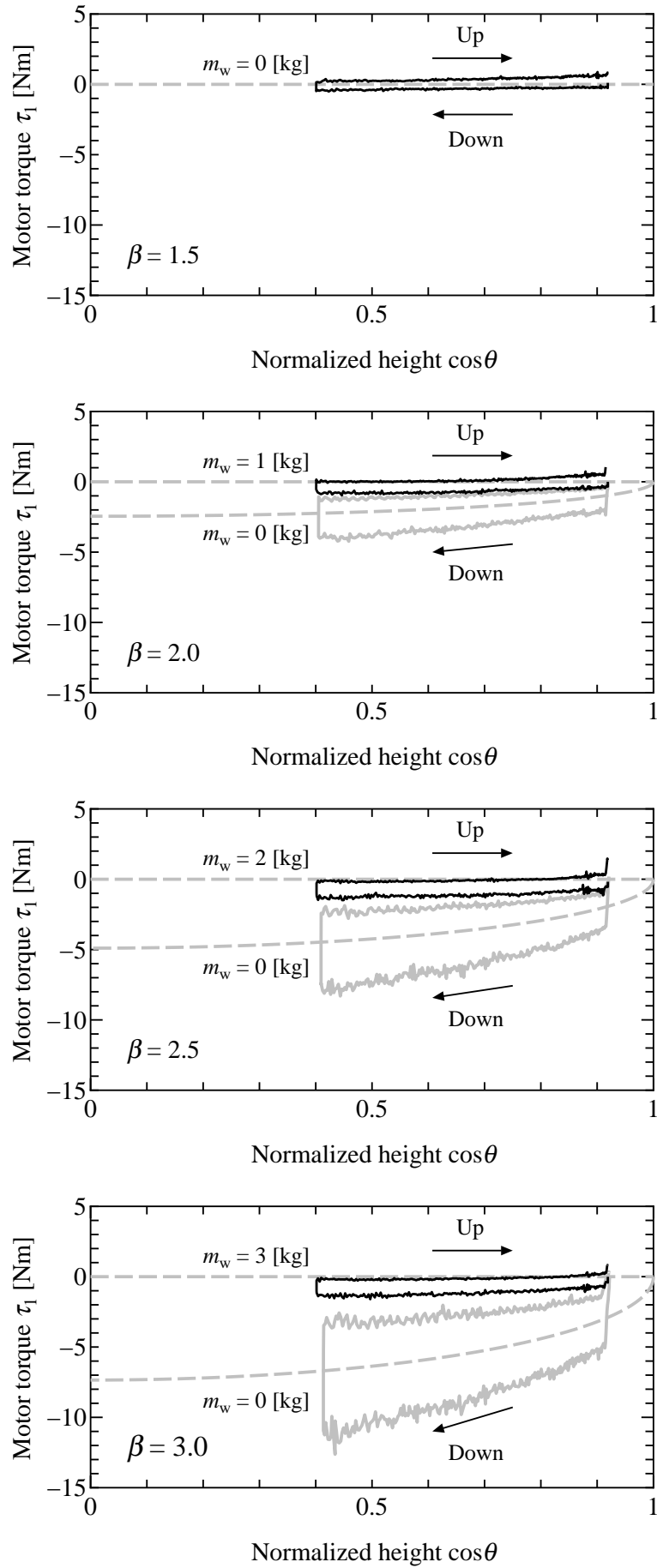
Figure 10. Lift motor torque vs. normalized height for $\beta = 1.5$, 2.0, 2.5, and 3.0
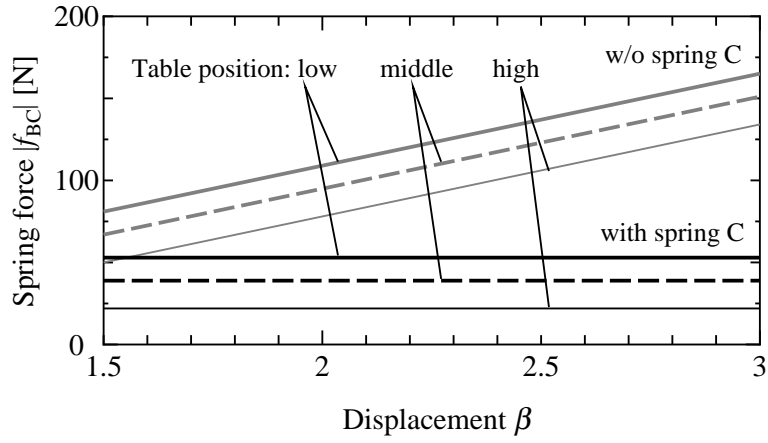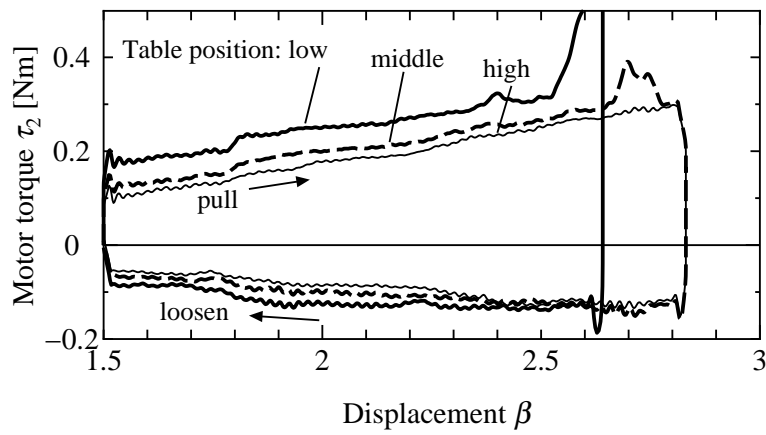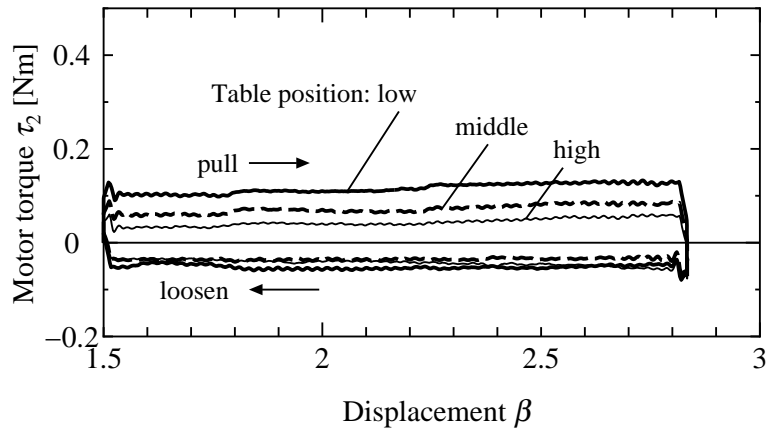
Figure 11. Theoretical adjustment force vs. displacement with and without spring C

(a) without spring C

(b) with spring C

Figure 12. Adjustment motor torque vs. displacement with and without spring C

Since the prototype uses a trapezoidal screw, which is non-backdrivable, to drive the slider, the direction of force and efficiency affect the motor torque. The experimental results are shown in Figs. 12(a) and 12(b). The vertical and horizontal axes indicate the torque of the adjustment motor and the displacement β, respectively.

Before the introduction of spring C, the motor torque increases in proportion to the displacement β ($s_{\text{Be}} = l_{\text{B}}(\beta - 1)$), as shown in Fig. 12(a). The motor torque also depends on the height of the table. When the table was at the low position, the motor torque was saturated, and the slider could not be pulled up to the predefined final displacement ($\beta = 2.8$).

Conversely, after the introduction of spring C, the motor torque is almost constant regardless of the displacement β, although it depends on the height of the table, as illustrated in Fig. 12(b). The adjustment motor torque was within 0.15 N·m even if the table position was low. Although using a high gear ratio allows a smaller motor for the adjustment, it will make the adjustment slower. The proposed method of this paper allows a smaller motor for the faster adjustment, as shown in the later experiments.

In this section, it was verified that the proposed VGCM-based scissor lift is effective and has the following characteristics.

(1) The introduction of springs A and B can reduce the required torque of the lift motor.
(2) Adjusting the displacement β of spring B can change the compensation force of the lift.
(3) The introduction of spring C can reduce the required torque of the adjustment motor.

5. Load Estimation and Self-Adjustment

5.1 Load Estimation

As shown in the previous section, if the work weight is known, the spring force assists the lift motor by adjusting the displacement β (s_{Be}). The work weight can be obtained from the production information in factories. However, if an unknown work weight is loaded on the lift table, the compensation force may not be balanced by the load. Therefore, to compensate for the unknown weight, a method of detecting the work weight is necessary, as considered in this section.

The easiest way to determine the work weight is to utilize a load cell on top of the table. However, load cells are generally weak against shock and are relatively costly. The compensation force does not have to perfectly correspond to the load if the torque of the lift motor is reduced. In this study, the estimation of the work weight is adopted based on the dynamic model of the lift.

The dynamics of the scissor lift are modeled as shown in Fig. 13. The equations of motion are written as

$$H(\theta)\ddot{\theta} + C(\theta,\dot{\theta})\dot{\theta} + G(\theta) + F\text{sgn}(\dot{\theta}) + D\dot{\theta} - \tau_k(\beta_0) = \tau_m \tag{18}$$

$$H(\theta) = I_{\text{A}} + m_{\text{A}}\left(l_{g\text{A}}^2 + (l_{\text{A}} - 2l_{g\text{A}})\,l_{\text{A}}\cos^2\theta\right) + I_{\text{B1}} + I_{\text{B2}} + I_{\text{B3}} + m_{\text{B1}}l_{g\text{B1}}^2 + m_{\text{B2}}l_{g\text{B2}}^2$$

$$+ m_{\text{B3}}\left((l_{g\text{B3}} + l_{\text{B}}/2)^2 - 2l_{\text{B}}l_{g\text{B3}}\cos^2\theta\right) + m_{\text{T}}l_{\text{A}}^2\sin^2\theta \tag{19}$$

$$C(\theta,\dot{\theta}) = \left((m_{\text{T}} - m_{\text{A}})l_{\text{A}}^2 + 2(m_{\text{A}}l_{\text{A}}l_{g\text{A}} + m_{\text{B3}}l_{\text{B}}l_{g\text{B3}})\right)\dot{\theta}\sin\theta\cos\theta \tag{20}$$

$$G(\theta) = -g\left((m_{\text{A}}l_{g\text{A}} + m_{\text{B1}}l_{g\text{B1}} + m_{\text{T}}l_{\text{A}})\sin\theta + (m_{\text{B2}}l_{g\text{B2}} + m_{\text{B3}}(l_{\text{B}}/2 - l_{g\text{B3}}))\cos\theta\right) \tag{21}$$

where, $H(\theta)\ddot{\theta}$ is the inertia term; $C(\theta,\dot{\theta})\dot{\theta}$ is the Coriolis and centrifugal term; $G(\theta)$ is the gravity term; $F\text{sgn}(\dot{\theta})$ and $D\dot{\theta}$ are the friction and viscosity terms of lift motor, respectively. $\tau_k(\beta)$ is the compensation torque of springs (7); and τ_m is the torque τ_1 of the lift motor.

The equation can be rewritten in the following form[30, 31]:

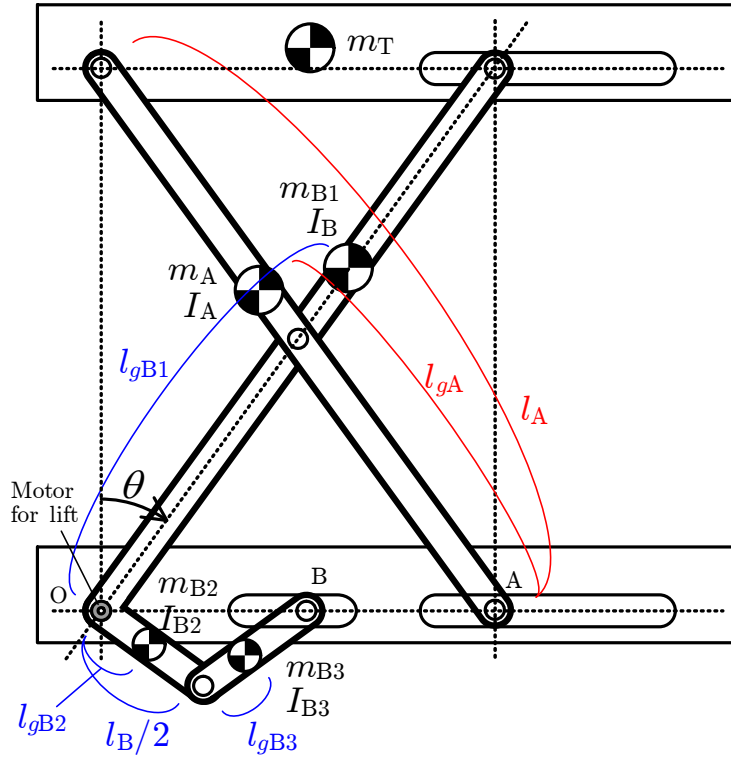$$Y(\theta,\dot{\theta},\ddot{\theta})\rho_0 = \tau_m \tag{22}$$

14

Figure 13. Dynamic model of scissor lift

where,

$$
Y(\theta,\dot{\theta},\ddot{\theta}) =
\begin{bmatrix}
\ddot{\theta} \\
\ddot{\theta}\sin^2\theta + \dot{\theta}^2\sin\theta\cos\theta \\
\ddot{\theta}\cos^2\theta - \dot{\theta}^2\sin\theta\cos\theta \\
\sin\theta\cos\theta \\
\sin\theta \\
\cos\theta \\
\mathrm{sgn}(\dot{\theta}) \\
\dot{\theta}
\end{bmatrix}^T
\tag{23}
$$

$$
\rho =
\begin{bmatrix}
I_A + I_{B1} + I_{B2} + I_{B3} + m_A l_{gA}^2 + m_{B1} l_{gB1}^2 \\
+ m_{B2} l_{gB2}^2 + m_{B3}\left(l_{gB3} + l_B/2\right)^2 \\
m_T l_A^2 \\
m_A l_A^2 - 2 m_A l_A l_{gA} - 2 m_{B3} l_B l_{gB3} \\
k_A l_A^2 - k_B l_B^2 \\
-g(m_A l_{gA} + m_{B1} l_{gB1} + m_T l_A) + \beta_0 k_B l_B^2 \\
-g\left(m_{B2} l_{gB2} + m_{B3}\left(l_B/2 - l_{gB3}\right)\right) \\
F \\
D
\end{bmatrix}.
\tag{24}
$$

$Y(\theta,\dot{\theta},\ddot{\theta})$ is generally called the regressor, and ρ_0 is a vector of parameters[30].

The position of the lift motor is controlled at a certain desired angle, angular velocity, and angular acceleration. The parameters ρ_0, which are considered to take constant values when the displacement is set to the constant as β_0, are identified from the experimental data of
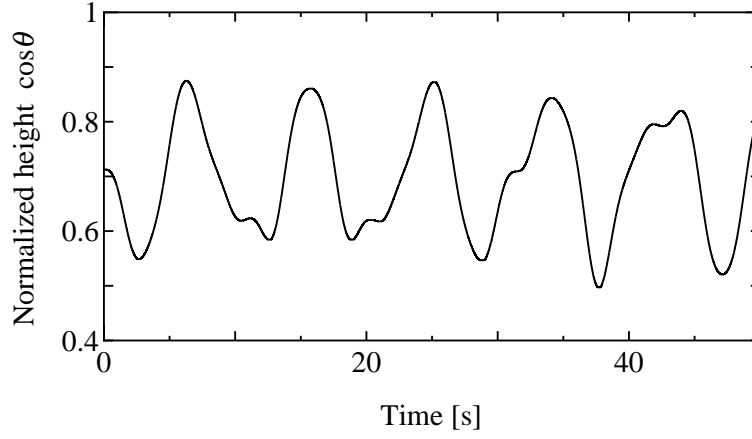
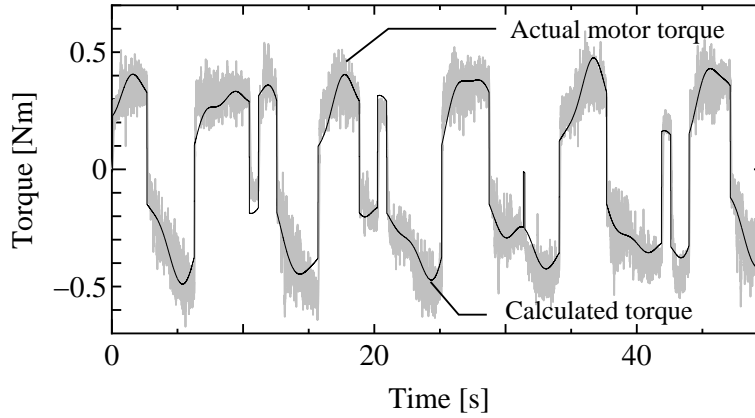Figure 14. Example of desired height of the table

Figure 15. Comparison of actual motor torque (gray) and torque calculated by identified parameters (black)

$Y_i(\theta_d, \dot{\theta}_d, \ddot{\theta}_d)$ and τ_{m_i} $(i = 0, \cdots, k)$ as

$$
\widehat{\rho}_0 = \begin{bmatrix} Y_0(\theta_d, \dot{\theta}_d, \ddot{\theta}_d) \\ Y_1(\theta_d, \dot{\theta}_d, \ddot{\theta}_d) \\ \vdots \\ Y_k(\theta_d, \dot{\theta}_d, \ddot{\theta}_d) \end{bmatrix}^+ \begin{bmatrix} \tau_{m\_0} \\ \tau_{m\_1} \\ \vdots \\ \tau_{m\_k} \end{bmatrix}
\tag{25}
$$

where $\widehat{\rho}_0$ indicates the identified vector with the initial displacement β_0 and $[\cdot]^+$ denotes the pseudoinversion of a matrix.

As a result of the identification, the following values are obtained:

$$
\widehat{\rho}_0 = [0.10, \, 0.17, \, -0.07, \, -0.17, \, 0.46, \, -0.38, \, 0.24, \, 0.74]^T .
\tag{26}
$$

As an example, the desired height of the lift table was given as shown in Fig. 14. The actual motor torque (command) τ_m and the torque calculated by the identified parameters $Y(\theta_d, \dot{\theta}_d, \ddot{\theta}_d)\widehat{\rho}_0$ are compared in Fig. 15. The gray and black lines express the actual and calculated motor torques, respectively. The calculated torque shows good agreement with the actual motor torque (the correlation coefficient is 0.96).

Next, the additional work weight must be estimated. It is assumed that the change in the gravity term is large and the change in the rest is relatively small when the weight is added.
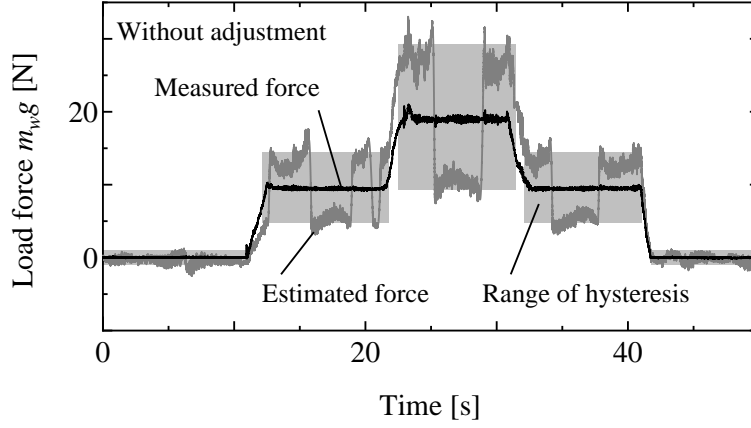
16

Figure 16. Measured and estimated load forces with the load applied to the table without adjustment

The related variable in the gravity term is the mass m_T of the table. The lifted mass becomes $m_T + m_W$ from m_T, where m_W is the added mass and generates the torque $\tau_w = m_W g l_A \sin\theta$. When the additional weight and the adjusted spring force are considered, the dynamics can be rewritten as the following equation:

$$Y(\theta, \dot{\theta}, \ddot{\theta})\rho_0 - \tau_k(\beta - \beta_0) = \tau_m + \tau_w. \tag{27}$$

Since the calculated torque showed good agreement with the actual torque as shown in Fig. 15, in the same manner as the disturbance observer, the additional work weight is estimated as

$$\hat{\tau}_w = \widehat{m_W g} l_A \sin\theta = Y(\theta_d, \dot{\theta}_d, \ddot{\theta}_d)\widehat{\rho}_0 - \tau_k(\beta - \beta_0) - \tau_m \tag{28}$$

$$\widehat{m_W g} = \frac{Y(\theta_d, \dot{\theta}_d, \ddot{\theta}_d)\widehat{\rho}_0 + (\beta - \beta_0)W\sin\theta - \tau_m}{l_A \sin\theta}. \tag{29}$$

During the motion shown in Fig. 14, a weight of 1 kg is loaded on the table at approximately 10 s. An additional weight of 1 kg (total weight of 2 kg) is loaded on the table at approximately 20 s. At approximately 30 and 40 s, the weights are unloaded one at a time. In this experiment, the displacement of the slider has not yet changed.

The experimental results are shown in Fig. 16. The black line represents the measured force due to the weight by the load cell. The gray line shows the estimated force based on (29).

In the estimated force, large errors are observed, which may be caused by the hysteresis shown in Figs. 9 and 10. The light gray bands in Fig. 16 represent the range of the hysteresis. In other words, the estimated force includes the influence of friction force depending on the load and the velocity (the direction of motion). It is expected that the estimation error can be reduced if the spring force is balanced by the weight.

5.2   *Self-Adjustment*

The displacement β of the slider is changed so that the compensation force is balanced with the estimated force $\widehat{m_W g}$. The desired displacement β_d of the slider is written as

$$\beta_d = \beta_0 + \frac{\widehat{m_W g}}{mg}. \tag{30}$$

Since the estimated load $\widehat{m_W g}$ may be noisy, a low-pass filter $\dfrac{1}{Ts+1}$, in which s is a Laplace operator, with a time constant $T = 0.5$ s is employed in the following experiments.
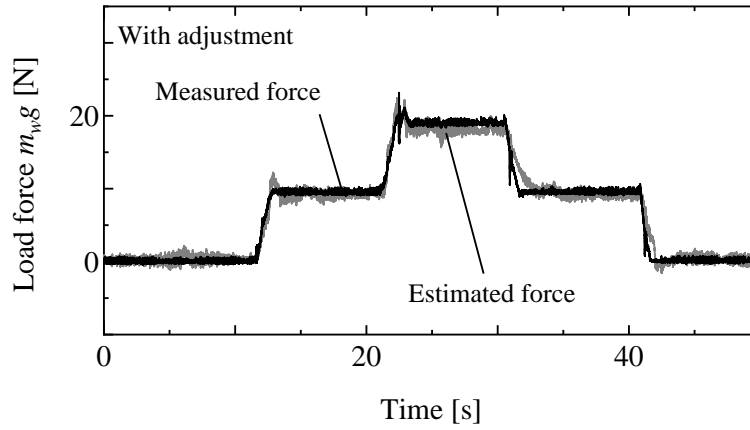
17

Figure 17. Measured and estimated load forces with the load applied to the table with adjustment
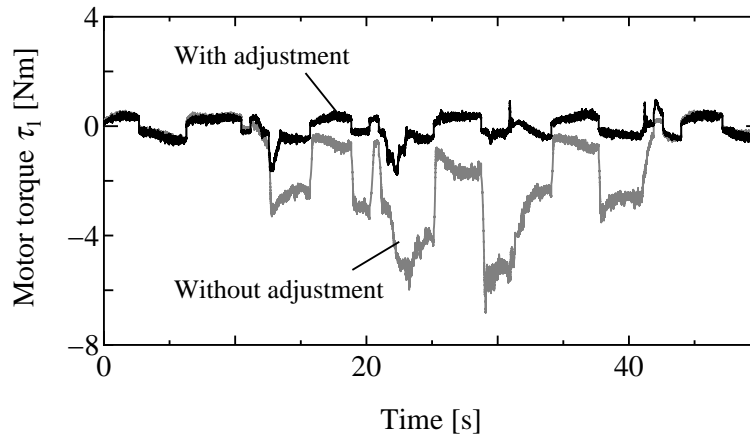

Figure 18. Lift motor torque with and without adjustment

The motion of the table is the same as that shown in Fig. 14. During the motion, the additional weights are loaded on the table as the same with the previous section. (a weight of 1 kg is loaded on the table at approximately 10 s. An additional weight of 1 kg is loaded at approximately 20 s. At approximately 30 and 40 s, the weights are unloaded one at a time.) The experimental results are shown in Fig. 17. The black line represents the measured force, and the gray line illustrates the estimated force using (29). In this case, the estimation agrees very well with the measurement. (the correlation coefficient is 0.99).

The torques of the lift motor with and without the adjustment of the compensation are shown in Fig. 18. When the additional weights were applied and the compensation force was not adjusted, the maximum torque of the lift motor was approximately 6 N·m for a weight of 2 kg. Conversely, when the compensation force was adjusted, the torque of the lift motor was within 1 N·m.

The displacement β during the motion is shown in Fig. 19. It changed immediately according to the estimated force shown in Fig. 17.

The torque of the adjustment motor is illustrated in Fig. 20. It was in almost the same range as that shown in Fig. 12(b).

6.   Conclusions

This paper proposed a scissor lift based on VGCM using three springs. A prototype was designed and fabricated. To evaluate the performance of the prototype, experiments were carried out.
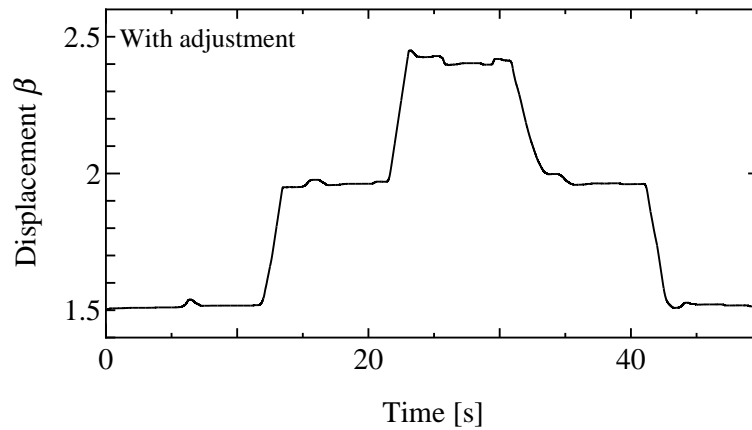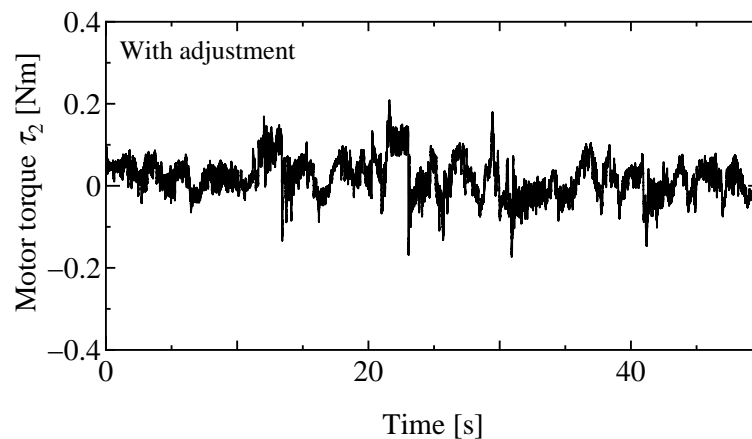
Figure 19. Displacement β with adjustment

Figure 20. Adjustment motor torque with adjustment

The results demonstrated that the developed scissor lift was in good agreement with the design specifications.

In addition, a load estimator was established based on the dynamic model of the scissor lift. A real-time self-adjustment method was proposed, and its effectiveness was experimentally verified.

Future studies may address the multiplication of the proposed scissor lift for larger heights and the magnification of the compensation force for industrial applications.

Disclosure statement

No potential conflict of interest was reported by the authors.

Notes on contributors

Naoyuki Takesue received BE and ME degrees from The University of Electro- Communications, respectively, in 1995 and 1997. In 2000, he received his PhD in Engineering from Osaka University. He joined Osaka University in 2000 and then joined Nagoya Institute of Technology in 2003. He joined Tokyo Metropolitan University in 2008 as an associate professor. His research interests include mechanism design, industrial applications, physically assistive robots, and aquatic robots.

Yosuke Komoda received his bachelor and master degrees in Engineering from Tokyo 5 Metropolitan University, respectively, in 2011 and 2013. He currently works at Isuzu Motors Ltd.

Hideyuki Murayama received his bachelor and master degrees in Engineering from Tohoku University, respectively, in 1995 and 1997. He joined Mitsubishi Electric Corporation in 1997 and joined Toyota Motor Corporation in 2003. He developed human cooperation robots for assembly operation at Partner Robot Division. He currently works at Production Engineering Development Division. He received the Technical Innovations Award from the Robotics Society of Japan in 2011 and the JSME Medal for New Technology from the Japan Society of Mechanical Engineers in 2012.

Kousyun Fujiwara joined Toyota Motor Corporation in 1973. He worked at General Assembly Engineering Division and developed human cooperation robots for assembly operation. He retired from Toyota Motor Corporation in 2015. He received the Technical Innovations Award from the Robotics Society of Japan in 2011 and the JSME Medal for New Technology from the Japan Society of Mechanical Engineers in 2012.

Hideo Fujimoto received the BE andDr Eng degrees from Nagoya University, Nagoya, Japan, in 1970 and 1982, respectively, all in mechanical engineering. He joined Nagoya Institute of Technology in 1972. He is currently a project professor and a Professor Emeritus at Nagoya Institute of Technology. His research interests include medical engineering, haptic engineering, and robotics. Fujimoto is a Fellow of the Japan Society of Mechanical Engineers. He was the recipient of the Best Paper Award for a paper presented at the 2000 Japan-USA Flexible Automation Symposium, the Best Paper Award at the Sixth Robotics Symposium, the Contribution Award from the System Integration Section, Society of Instrument and Control Engineers, and the Great Contribution Award from the Production System Section, the Japan Society of Mechanical Engineers, in 2002.

References

[1] H. S. Kim and J. B. Song: Multi-DOF Counterbalance Mechanism for a Service Robot Arm, IEEE/ASME Trans. Mechatronics, Vol.19, No.6, pp.1756–1763, 2014.

[2] S. Mahalingam and A. M. Sharan: The Optimal Balancing of the Robotic Manipulators, Proc. 1986 IEEE Int. Conf. Robot. Autom., pp.828–835, 1986, San Francisco, USA.

[3] J. P. Whitney and J. K. Hodgins: A Passively Safe and Gravity-counterbalanced Anthropomorphic Robot Arm, Proc. 2014 IEEE Int. Conf. Robot. Autom., pp.6168–6173, 2014, Hong Kong, China.

[4] A. Kawamura, T. Hisatsune, K. Matsusaka, M. Uemura and S. Kawamura: Adaptive Motion Control of a Robotic Arm with Movable Counterweights, Proc. 2014 IEEE/ASME Int. Conf. on Advanced Intelligent Mechatronics, pp.882–887, 2014, Besançon, France.

[5] R. H. Nathan: A Constant Force Generation Mechanism, Trans. ASME J. Mechanisms, Transmissions, and Automation in Design, Vol.107, No.4, pp.508–512, 1985.

[6] D. A. Streit and B. J. Gilmore: 'Perfect' Spring Equilibrators for Rotatable Bodies, Trans. ASME J. Mechanisms, Transmissions, and Automation in Design, Vol.111, No.4, pp.451–458, 1989.

[7] T. Rahman, R. Ramanathan, R. Seliktar and W. Harwin: A Simple Technique to Passively Gravity-balance Articulated Mechanism, ASME Trans. on Mechanisms Design, Vol.117, No.4, pp.655–658, 1995.

[8] M. J. French and M. B. Widden: The Spring-and-lever Balancing Mechanism, George Carwardine and the Anglepoise Lamp, Proc. of the Institution of Mechanical Engineers, Part C: J. of Mechanical Engineering Science, Vol.214, No.3, pp.501–508, 2000.

[9] T. Morita, F. Kuribara, Y. Shiozawa and S. Sugano: A Novel Mechanism Design for Gravity Compensation in Three Dimensional Space, Proc. 2003 IEEE/ASME Int. Conf. on Advanced Intelligent Mechatronics, pp.163–168, 2003, Kobe, Japan.

[10] J. M. Hervé: Design of Spring Mechanisms for Balancing the Weight of Robots, Proc. the Sixth CISM-IFToMM Symposium on Theory and Practice of Robots and Manipulators, pp.564–567, 1986, Cracow, Poland.

[11] T. Nakayama, Y. Araki and H. Fujimoto: A New Gravity Compensation Mechanism for Lower Limb Rehabilitation, Proc. 2009 IEEE Int. Conf. on Mechatronics and Automation, pp.943–948, 2009, Changchun, China.

[12] N. Ulrich and V. Kumar: Passive Mechanical Gravity Compensation for Robot Manipulators, Proc. 1991 IEEE Int. Conf. Robot. Autom., pp.1536–1541, 1991, Sacramento, California.

[13] G. Endo, H. Yamada, A. Yajima, M. Ogata and S. Hirose: A Passive Weight Compensation Mechanism with a Non-Circular Pulley and a Spring, Proc. 2010 IEEE Int. Conf. Robot. Autom., pp.3843–3848, 2010, Anchorage, USA.

[14] Kenan Koser: A Cam Mechanism for Gravity-balancing, Mechanics Research Communications, Vol.36, Iss.4, pp.523–530, 2009.

[15] K. Kaneoka, N. Nakagawa and Y. Sekiguchi: Design and Development of Spring Link Mechanism with the Constant Repulsive Force Characteristics Proc. the First Int. Conf. on Design Engineering and Science 2005, pp.305–310, 2005, Vienna, Austria.

[16] N. Nakagawa, T. Okuno and Y. Sekiguchi: A Study on Improvement of Constant Repulsive Force Characteristic, Trans. Japan Society of Mechanical Engineers, Series C, Vol.74, No.739, pp.536–541, 2008. (in Japanese)

[17] T. Nakayama, Y. Araki and H. Fujimoto: Development of Mechanical Gravity Compensation System for Heavy Load, Proc. the 11th SICE System Integration Division Annual Conference, pp.1483–1486, 2010. (in Japanese)

[18] W. D. van Dorsser, R. Barents, B. M. Wisse and J. L. Herder: Balancing Device, Patent NL1029989C, 2005.

[19] W. D. van Dorsser, R. Barents, B. M. Wisse and J. L. Herder: Energy Free Adjustment of Gravity Equilibrators with Application in a Mobile Arm Support, Proc. ASME Design Engineering Technical Conferences and Computers and Information in Engineering Conference, DETC2006-99745, 2006, Philadelphia, USA.

[20] B. M. Wisse, W. D. van Dorsser, R. Barents and J. L. Herder: Energy-free Adjustment of Gravity Equilibrators Using the Virtual Spring Concept, Proc. 2007 IEEE Int. Conf. on Rehabilitation Robotics, pp.742–750, 2007, Noordwijk, Netherlands.

[21] W. D. van Dorsser, R. Barents, B. M. Wisse, M. Schenk and J. L. Herder: Energy-free Adjustment of Gravity Equilibrators by Adjusting the Spring Stiffness, Proc. IMechE, Vol.222, Part C, J. of Mechanical Engineering Science, pp.1839–1846, 2008.

[22] R. Barents, M. Schenk, W. D. Dorsser, B. M. Wisse, and J. L. Herder: Spring-to-spring balancing as energy-free adjustment method in gravity equilibrators, Proc. ASME 2009 Int. Design Engineering Technical Conferences, DETC2009-86770, 2009, San Diego, USA.

[23] Eugene F. Duval: Mechanical Arm Including A Counter-balance, Patent US 7798035 B2, 2010.

[24] Tao Liu and Jian Sun: Simulative Calculation and Optimal Design of Scissor Lifting Mechanism, Proc. 2009 Chinese Control and Decision Conference, pp.2079–2082, 2009, Guilin, China.

[25] R. G. Dong, C. S. Pan, J. J. Hartsell, D. E. Welcome, T. Lutz, A. Brumfield, J. R. Harris, J. Z. Wu, B. Wimer, V. Mucino and K. Means: An Investigation on the Dynamic Stability of Scissor Lift, Open Journal of Safety Science and Technology, Vol.2, No.1, pp.8–15, 2012.

[26] M. T. Islam, C. Yin, S. Jian and L. Rolland: Dynamic Analysis of Scissor Lift Mechanism through Bond Graph Modeling, Proc. 2014 IEEE/ASME Int. Conf. on Advanced Intelligent Mechatronics, pp.1393–1399, 2014, Besançon, France.

[27] D. L. Platus: Negative-stiffness-mechanism Vibration Isolation Systems, Proc. SPIE 1619, Vibration Control in Microelectronics, Optics, and Metrology, pp.44–54, 1992, San Jose, USA.

[28] T. Mizuno, T. Toumiya and M. Takasaki: Vibration Isolation System Using Negative Stiffness, JSME International Journal, Series C, Vol.46, No.3, pp.807–812, 2003.

[29] N. Takesue, T. Ikematsu, H. Murayama and H. Fujimoto: Design and Prototype of Variable Gravity Compensation Mechanism (VGCM), J. of Robotics and Mechatronics, Vol.23, No.2, pp.249–257, 2011.

[30] R. Ortega and M. W. Spong: Adaptive Motion Control of Rigid Robots: A Tutorial, Proc. IEEE Conf. on Decision and Control, pp.1575–1584, 1988, Austin, USA.

[31] J. J. E. Slotine and W. Li: Adaptive Manipulator Control: A Case Study, IEEE Trans. Automat. Contr., Vol.AC-33, No.11, pp.995–1003, 1988.